Diffraction at HERA, the Tevatron and the LHC

C. Royon

DAPNIA/Service de physique des particules, CEA/Saclay, 91191 Gif-sur-Yvette cedex, France

In these lectures, we present and discuss the most recent results on inclusive diffraction from the HERA and Tevatron colliders and give the prospects for the future at the LHC. Of special interest is the exclusive production of Higgs boson and heavy objects (W, top, stop pairs) which will require a better understanding of diffractive events and the link between ep and hadronic colliders, as well as precise measurements and analyses of inclusive diffraction at the LHC in particular to constrain further the gluon density in the pomeron.

In these lectures, we describe the most recent results on inclusive diffraction at HERA, as well as diffractive results from the Tevatron. We finish the lecture by discussing the prospects of diffractive physics at the LHC.

1. Experimental definition of diffraction

In this section, we discuss the different experimental ways to define diffraction. As an example, we describe the methods used by the H1 and ZEUS experiments at HERA, DESY, Hamburg in Germany.

1.1. The rapidity gap method

HERA is a collider where electrons of 27.6 GeV collide with protons of 920 GeV. A typical event as shown in the upper plot of Fig. 1 is $ep \to eX$ where electron and jets are produced in the final state. We notice that the electron is scattered in the H1 backward detector[1] (in green) whereas some hadronic activity is present in the forward region of the detector (in the LAr calorimeter and in the forward muon detectors). The proton is thus completely destroyed and the interaction leads to jets and proton remnants directly observable in the detector. The fact that much energy is observed

[1] At HERA, the backward (resp. forward) directions are defined as the direction of the outgoing electron (resp. proton).

in the forward region is due to colour exchange between the scattered jet and the proton remnants. In about 10% of the events, the situation is completely different. Such events appear like the one shown in the bottom plot of Fig. 1. The electron is still present in the backward detector, there is still some hadronic activity (jets) in the LAr calorimeter, but no energy above noise level is deposited in the forward part of the LAr calorimeter or in the forward muon detectors. In other words, there is no color exchange between the proton and the produced jets. As an example, this can be explained if the proton stays intact after the interaction.

This experimental observation leads to the first definition of diffraction: request a rapidity gap (in other words a domain in the forward detectors where no energy is deposited above noise level) in the forward region. For example, the H1 collaboration requests no energy deposition in the rapidity region $3.3 < \eta < 7.5$ where η is the pseudorapidity. Let us note that this approach does not insure that the proton stays intact after the interaction, but it represents a limit on the mass of the produced object $M_Y < 1.6$ GeV. Within this limit, the proton could be dissociated. The adavantage of the rapidity gap method is that it is quite easy to implement and it has a large acceptance in the diffractive kinematical plane.

1.2. Proton tagging

The second experimental method to detect diffractive events is also natural: the idea is to detect directly the intact proton in the final state. The proton loses a small fraction of its energy and is thus scattered at very small angle with respect to the beam direction. Some special detectors called roman pots can be used to detect the protons close to the beam. The basic idea is simple: the roman pot detectors are located far away from the interaction point and can move close to the beam, when the beam is stable, to detect protons scattered at vary small angles. The inconvenience is that the kinematical reach of those detectors is much smaller than with the rapidity gap method. On the other hand, the advantage is that it gives a clear signal of diffraction since it measures the diffracted proton directly.

A scheme of a roman pot detector as it is used by the H1 or ZEUS experiment is shown in Fig. 2. The beam is the horizontal line at the upper part of the figure. The detector is located in the pot itself and can move closer to the beam when the beam is stable enough (during the injection period, the detectors are protected in the home position). Step motors allow to move the detectors with high precision. A precise knowledge of the detector position is necessary to reconstruct the transverse momentum of the scattered proton and thus the diffractive kinematical variables. The detectors are placed in a secondary vaccuum with respect to the beam one.

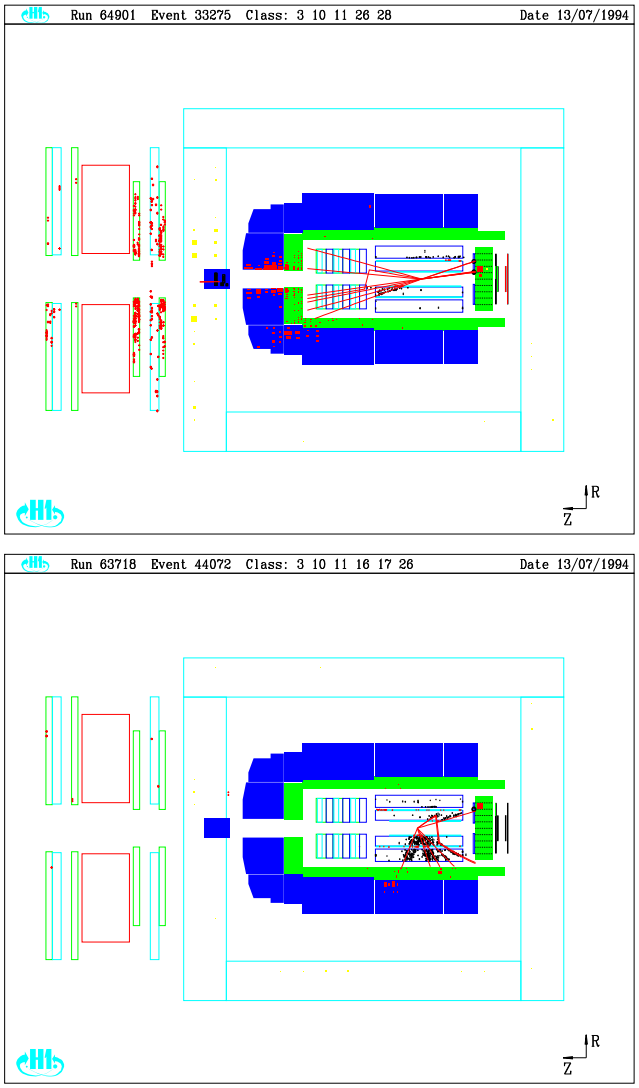

1

Fig. 1. "Usual" and diffractive events in the H1 experiment.

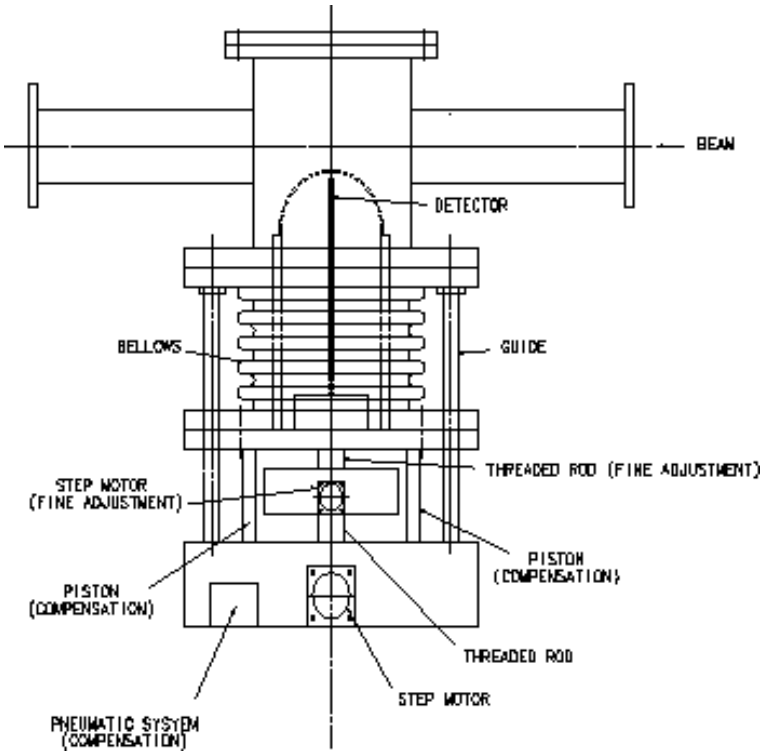

Fig. 2. Scheme of a roman pot detector.

1.3. The M_X method

The third method used at HERA mainly by the ZEUS experiment is slightly less natural. It is based on the fact that there is a different behaviour in $\log M_X^2$ where M_X is the total invariant mass produced in the event either for diffractive or non diffractive events. For diffractive events $d\sigma_{diff}/dM_X^2 = (s/M_X^2)^{\alpha-1} = const.$ if $\alpha \sim 1$ (which is the case for diffractive events). The ZEUS collaboration performs some fits of the $d\sigma/dM_X^2$ distribution:

$$\frac{d\sigma}{dM_X^2} = D + c\exp(b\log M_X^2) \tag{1}$$

as illustrated in Fig. 3. The usual non diffractive events are exponentially suppressed at high values of M_X. The difference between the observed $d\sigma/dM_X^2$ data and the exponential suppressed distribution is the diffractive event contribution. This method, although easy to implement, presents the inconvenience that it relies strongly on the assumption of the exponential suppression of non diffractive events.

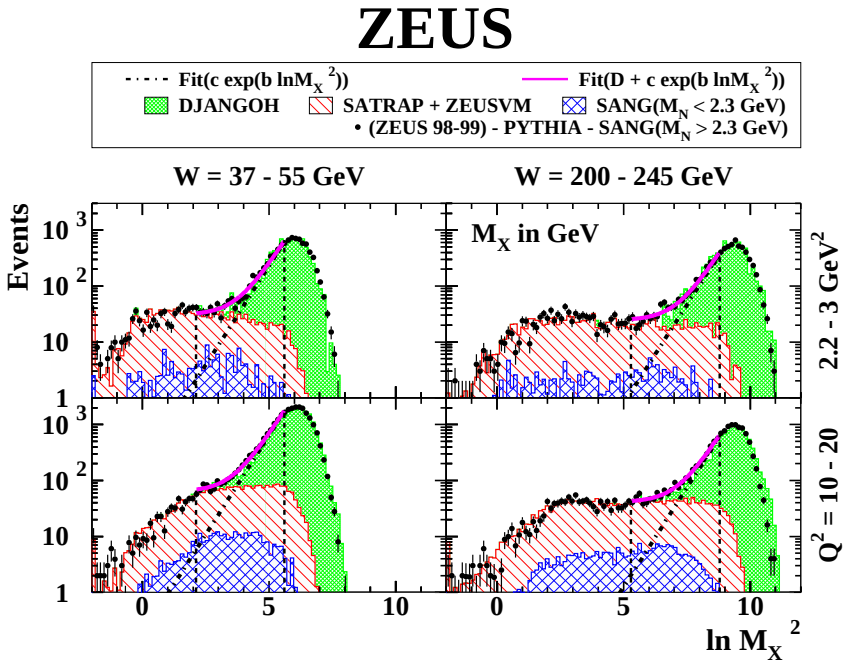

Fig. 3. Illustration of the M_X method used by the ZEUS collaboration to define diffractive events.

1.4. Diffractive kinematical variables

After having described the different experimental definitions of diffraction at HERA, we will give the new kinematical variables used to characterise diffraction. A typical diffractive event is shown in Fig. 4 where $ep \to epX$ is depicted. In addition to the usual deep inelastic variables, Q^2 the transfered energy squared at the electron vertex, x the fraction of the proton momentum carried by the struck quark, $W^2 = Q^2(1/x - 1)$ the total energy in the final state, new diffractive variables are defined: x_P is the momentum fraction of the proton carried by the colourless object called the pomeron, and β the momentum fraction of the pomeron carried by the interacting parton inside the pomeron if we assume the pomeron to be made of quarks and gluons:

$$x_P \; = \; \xi = \frac{Q^2 + M_X^2}{Q^2 + W^2} \tag{2}$$

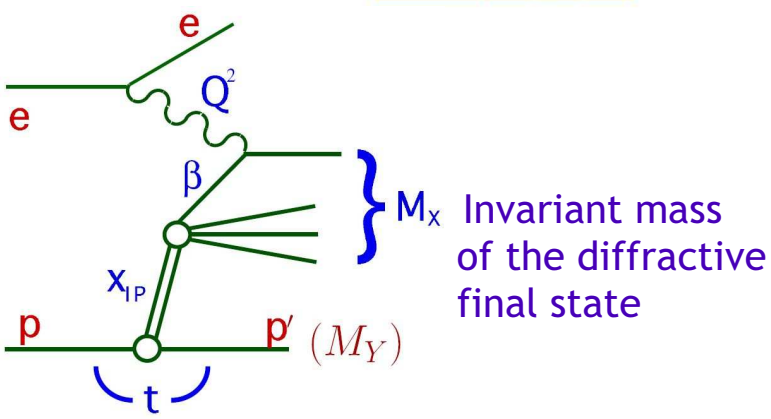

Fig. 4. Scheme of a diffractive event at HERA.

$$\beta = \frac{Q^2}{Q^2 + M_X^2} = \frac{x}{x_P}. \tag{3}$$

2. Diffractive structure function measurement at HERA

2.1. Diffractive factorisation

In the following diffractive structure function analysis, we distinguish two kinds of factorisation at HERA. The first factorisation is the QCD hard scattering collinear factorisation at fixed x_P and t (see left plot of Fig. 5) [1], namely

$$d\sigma(ep \to eXY) = f_D(x, Q^2, x_P, t) \times d\hat{\sigma}(x, Q^2) \tag{4}$$

where we can factorise the flux f_D from the cross section $\hat{\sigma}$. This factorisation was proven recently, and separates the γq coupling to the interaction with the colourless object.

The Regge factorisation at the proton vertex allows to factorise the (x_P, t) and (β, Q^2) dependence, or in other words the hard interaction from the pomeron coupling to the proton (see right plot of Fig. 5).

2.2. Measurement of the diffractive proton structure function

The different measurements are performed using the three different methods to define diffractive events described in the first section. As an example,

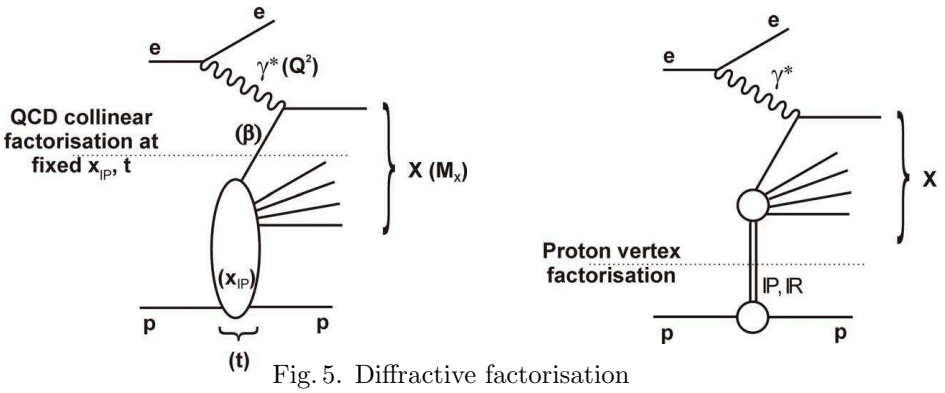

Fig. 5. Diffractive factorisation

the H1 collaboration measures the diffractive cross section σ^D using the rapidity gap method:

$$\frac{d^3\sigma^D}{dx_P dQ^2 d\beta} = \frac{2\pi\alpha_{em}^2}{\beta Q^4}\left(1 - y + \frac{y^2}{2}\right)\sigma_r^D(x_P, Q^2, \beta) \tag{5}$$

where σ_r^D is the reduced diffractive cross section. The measurement [2] is presented in Fig. 6. We notice that the measurement has been performed with high precision over a wide kinematical domain: $0.01 < \beta < 0.9$, $3.5 < Q^2 < 1600$ GeV^2, $10^{-4} < x_P < 5.10^{-2}$. The data are compared to the result of a QCD fit which we will discuss in the following.

The rapidity gap data are also compared with the data obtained either using the M_X method or the one using proton tagging in roman pot detectors. Since they do not correspond exactly to the same definition of diffraction, a correction factor of 0.85 must be applied to the ZEUS M_X method to be compared to the rapidity gap one (this factor is due to the fact that the two methods correspond to two different regions in M_Y, namely $M_Y < 1.6$ GeV for H1 and $M_Y < 2.3$ GeV for ZEUS). It is also possible to measure directly in the H1 experiment the ratio of the diffractive structure function measurements between the rapidity gap and the proton tagging methods as illustrated in Fig. 7. Unfortunately, the measurement using the proton tagging method is performed only in a restricted kinematical domain. No kinematical dependence has been found within uncertainties for this ratio inside this kinematical domain (see Fig. 7 for the β and Q^2 dependence, and Ref. [4] for the x_P dependence as well). Note that the ratio could still be depending on β and Q^2 outside the limited domain of measurement.

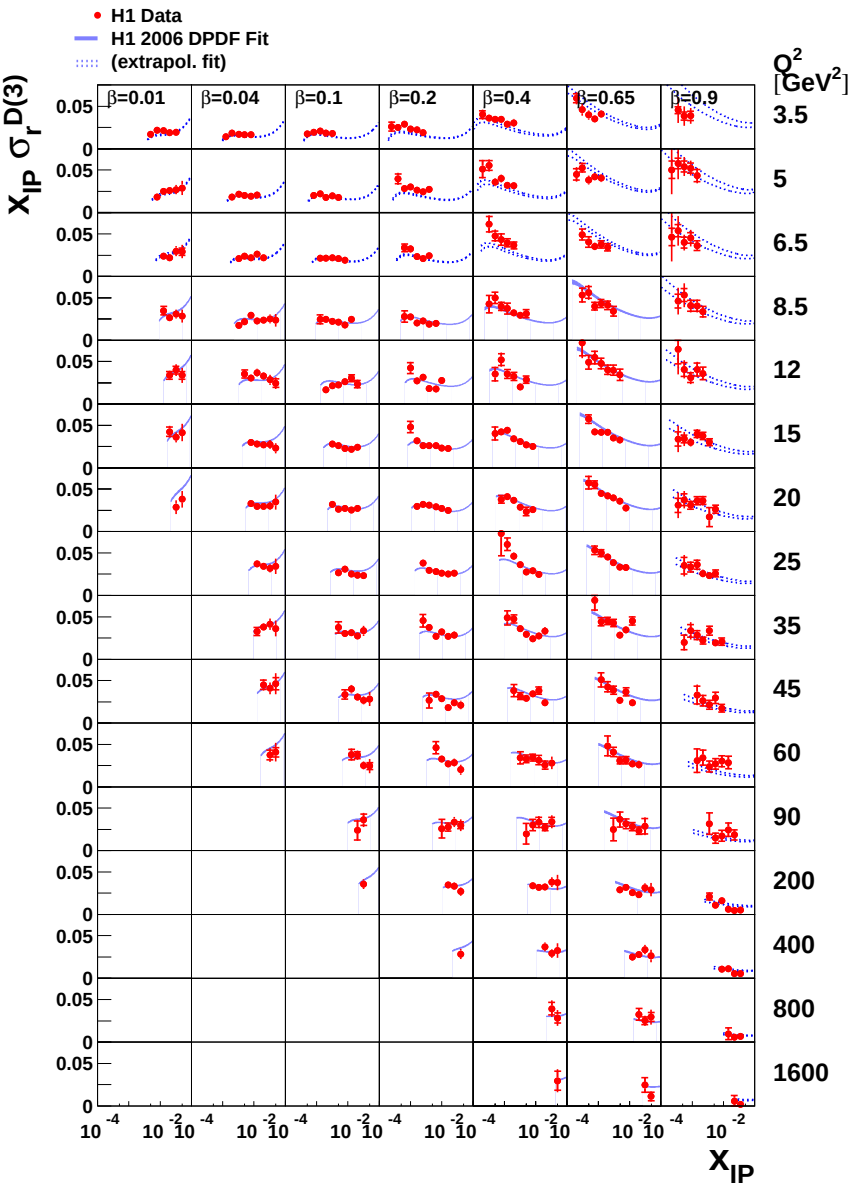

Fig. 6. Measurement of the diffractive structure function by the H1 collaboration

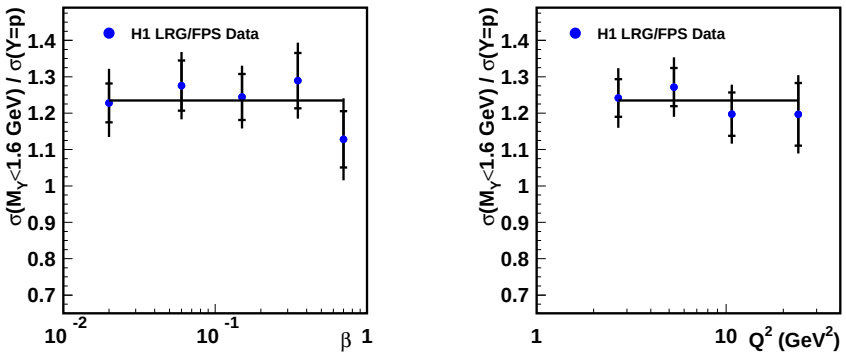

Fig. 7. Measurement of the ratio of the diffractive structure function between the rapidity gap and the proton tagging methods (H1 experiment).

2.3. QCD analysis of the diffractive structure function measurement

As we mentionned already, according to Regge theory, we can factorise the (x_P, t) dependence from the (β, Q^2) one. The first diffractive structure function measurement from the H1 collaboartion [5] showed that this assumption was not true. The natural solution as observed in soft physics was that two different trajectories, namely pomeron and secondary reggeon, were needed to describe the measurement, which lead to a good description of the data. The diffractive structure function then reads:

$$F_2^D \sim f_p(x_P)(F_2^D)_{Pom}(\beta, Q^2) + f_r(x_P)(F_2^D)_{Reg}(\beta, Q^2) \tag{6}$$

where f_p and f_r are the pomeron and reggeon fluxes, and $(F_2^D)_{Pom}$ and $(F_2^D)_{Reg}$ the pomeron and reggeon structure functions. The flux parametrisation is predicted by Regge theory:

$$f(x_P, t) = \frac{e^{B_P t}}{x_P^{2\alpha_P(t)-1}} \tag{7}$$

with the following pomeron trajectory

$$\alpha_P(t) = \alpha_P(0) + \alpha'_P t. \tag{8}$$

The t dependence has been obtained using the proton tagging method, and the following values have been found: $\alpha'_P = 0.06^{+0.19}_{-0.06}$ GeV^{-2}, $B_P =$

$5.5^{+0.7}_{-2.0}$ GeV^{-2} (H1). Similarly, the values of $\alpha_P(0)$ have been measured using either the rapidity gap for H1 or the M_X method for ZEUS in the QCD fit described in the next paragraph [6, 2]. The Reggeon parameters have been found to be $\alpha'_R = 0.3$ GeV^{-2}, $B_R = 1.6$ GeV^{-2} (H1). The value of $\alpha_R(0)$ has been determined from rapidity gap data and found to be equal to 0.5. Since the reggeon is expected to have a similar $q\bar{q}$ structure as the pion and the data are poorly sensitive to the structure function of the secondary reggeon, it was assumed to be similar to the pion structure with a free normalisation.

The next step is to perform Dokshitzer Gribov Lipatov Altarelli Parisi (DGLAP) [7] fits to the pomeron structure function. If we assume that the pomeron is made of quarks and gluons, it is natural to check whether the DGLAP evolution equations are able to describe the Q^2 evolution of these parton densities. As necessary for DGLAP fits, a form for the input distributions is assumed at a given Q_0^2 and is evolved using the DGLAP evolution equations to a different Q^2, and fitted to the diffractive structure function data at this Q^2 value. The form of the distribution at Q_0^2 has been chosen to be:

$$\beta q = A_q \beta^{B_q} (1-\beta)^{C_q} \quad (9)$$

$$\beta G = A_g (1-\beta)^{C_g}, \quad (10)$$

leading to three (resp. two) parameters for the quark (resp. gluon) densities. At low β, the evolution is driven by $g \to q\bar{q}$ while $q \to qg$ becomes more important at high β. All diffractive data with $Q^2 > 8.5$ GeV^2 and $\beta < 0.8$ have been used in the fit [2, 6] (the high β points being excluded to avoid the low mass region where the vector meson resonances appear). This leads to a good description of all diffractive data included in the fit.

The DGLAP QCD fit allows to get the parton distributions in the pomeron as a direct output of the fit, and is displayed in Fig. 8 as a blue shaded area as a function of β. We first note that the gluon density is much higher than the quark one, showing that the pomeron is gluon dominated. We also note that the gluon density at high β is poorly constrained which is shown by the larger shaded area.

Another fit was also performed by the H1 collaboration imposing $C_g = 0$. While the fit quality is similar, the gluon at high β is quite different, and is displayed as a black line in Fig. 8 (z is the equivalent of β for quarks). This shows further that the gluon is very poorly constrained at high β and some other data sets such as jet cross section measurements are needed to constrain it further.

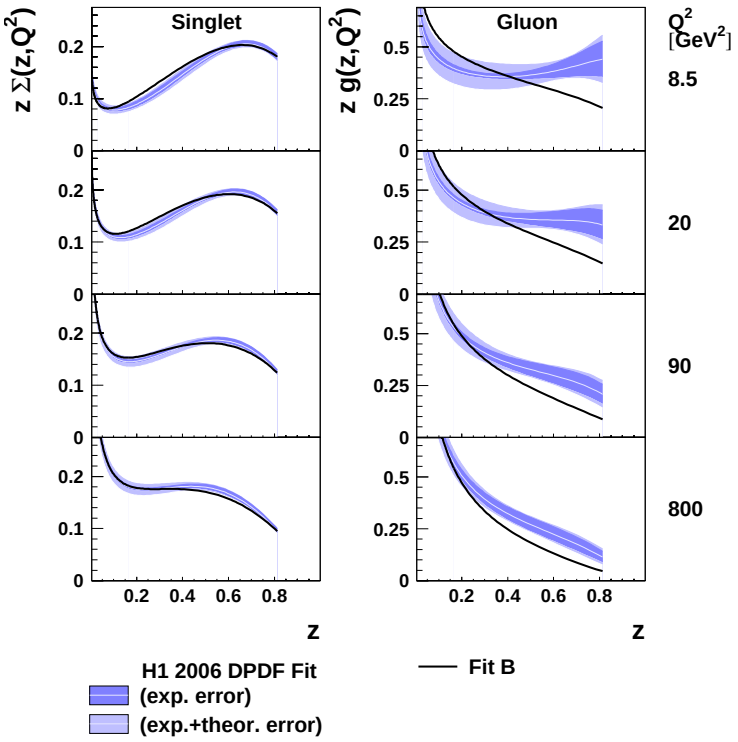

Fig. 8. Extraction of the parton densities in the pomeron using a DGLAP NLO fit (H1 collaboration).

2.4. QCD fits using diffractive structure function and jet cross section measurements

In this section, we describe combined fits using diffractive structure function and jet cross section data to further constrain the gluon at high β. First, it is possible to compare the diffractive dijet cross section measurements with the predictions using the gluon and quark densities from the QCD fits described in the previous section. The comparison [2] shows a discrepancy between the measurement and the expectation from the QCD fit by about a factor 2 at high β. This motivates the fact that it is important to add the jet cross section data to the inclusive structure function measure-

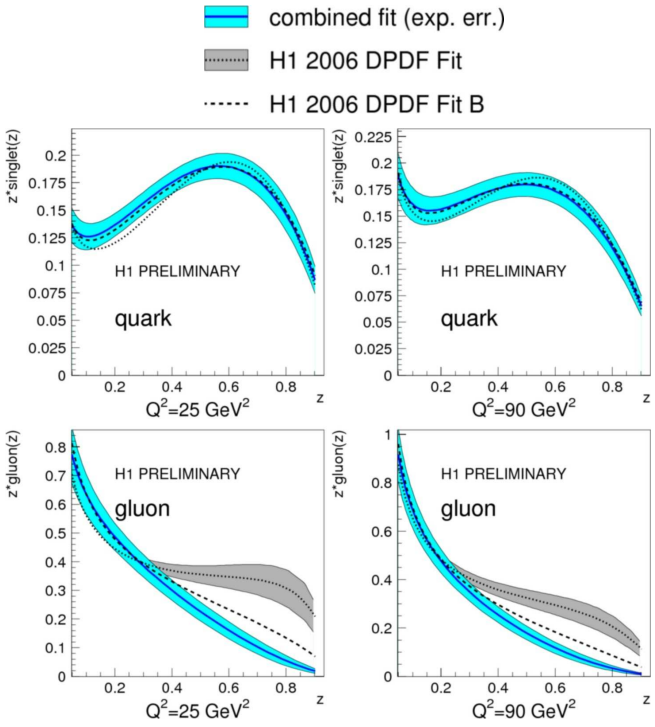

Fig. 9. Extraction of the parton densities in the pomeron using a DGLAP NLO fit (H1 collaboration). The blue shaded area shows the results after including both the diffractive structure function and the dijet cross section measurements into the QCD DGLAP fit.

ment in the QCD fit to further constrain the gluon density at high β. The new parton distributions are shown in Fig. 9 as a blue shaded area. The comparison between the jet cross section measurements and the prediction from the QCD fits are in good agreement as shown in Fig. 10. The present uncertainty is of the order of 50% at high β.

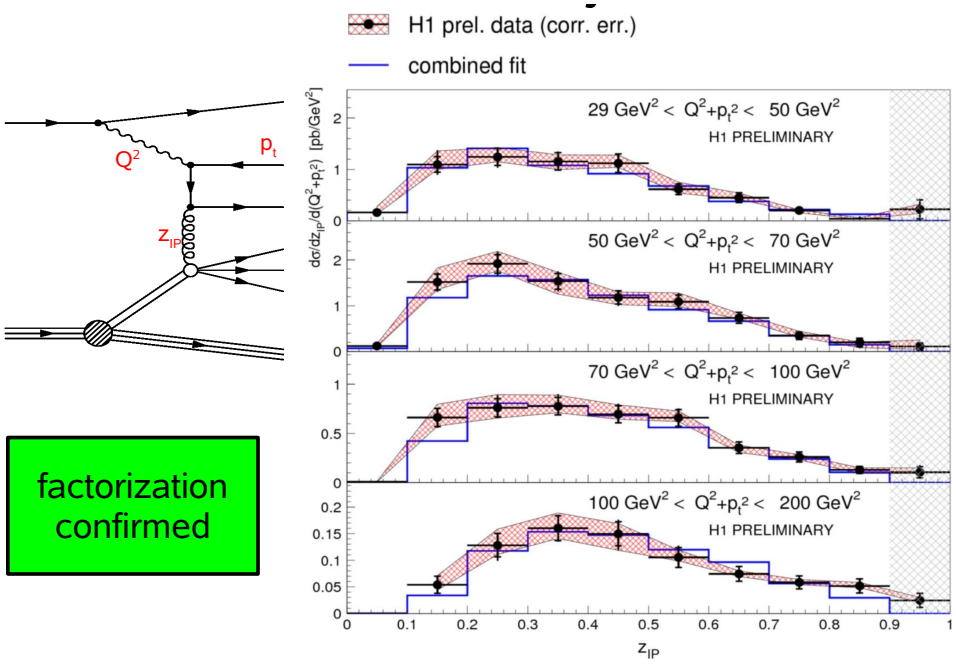

Fig. 10. Comparison between the H1 QCD diffractive fit based on diffractive structure function and dijet data and the dijet data.

2.5. Other models describing inclusive diffraction at HERA

Many different kinds of models can be used to describe inclusive diffraction at HERA, and we will describe here only the results based on the two gluon model [8]. Other models of interest such as the BFKL dipole model [9] or the saturation model [10] are described in Ref. [6] as well as the results of the fits to the diffractive data. Due to the lack of time, we cannot describe them in these lectures.

The 2-gluon model [8] starts from the image of a perturbative pomeron made of two gluons and coupled non perturbatively to the proton. As shown in Fig. 11, there are three main contributions to the diffractive structure function, namely the $q\bar{q}$ transverse, $q\bar{q}g$ (neglecting higher order Fock states) and the $q\bar{q}$ longitudinal terms. Contrary to the QCD fits described in the previous section, there is no concept of diffractive PDFs in this approach. The β-dependence of the structure function is motivated by some general features of QCD-parton model calculations: at small β the spin 1/2 (quark) exchange in the $q\bar{q}$ production leads to a behaviour $\sim \beta$, whereas the spin 1

$$x_{\mathbb{P}} F_2^{D(3)} = c_T \cdot F^T_{q\bar{q}} + c_L \cdot F^L_{q\bar{q}} + c_g \cdot F^T_{q\bar{q}g}$$

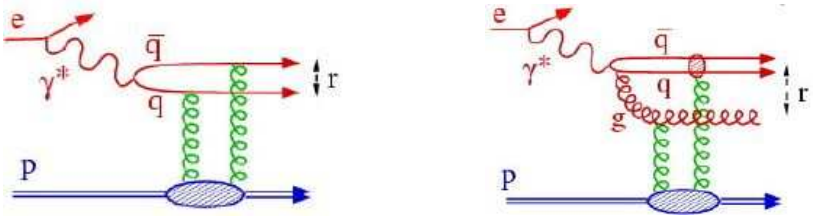

Fig. 11. Schematic view of the 2 gluon model [8].

(gluon) exchange in the $q\bar{q}g$ term corresponds to β^0. For large β, perturbative QCD leads to $1-\beta$ and $(1-\beta)^0$ for the transverse and longitudinal $q\bar{q}$ terms respectively. Concerning the Q^2 dependence, the longitudinal term is a higher twist one. Finally, the dependence on x_P cannot be obtained from perturbative QCD and therefore is left free. An additional sub-leading trajectory (secondary reggeon) has to be parametrised from soft physics and is added to the model as for the DGLAP based fit to describe H1 data.

The 2-gluon model leads to a good description of both ZEUS and H1 data. As an example, the comparison of the ZEUS M_X data [3] in different x_P and Q^2 bins as a function of β with the 2-gluon model is given in Fig. 12 where we note the good agreement between the model and the data. Fig. 12 also describes independently the three components of the model, namely the tranverse $q\bar{q}$ one which dominates at medium β, the $q\bar{q}g$ one at low β, and the longitudinal higher twist $q\bar{q}$ one at high β.

3. Diffraction at the Tevatron

The Tevatron is a $p\bar{p}$ collider located close to Chicago at Fermilab, USA. It is presently the collider with the highest center-of-mass energy of about 2 TeV. Two main experiments are located around the ring, DØ and CDF. Both collaborations have accumulated a luminosity of the order of 1.5 fb^{-1} with an efficiency of about 85%.

3.1. Diffractive kinematical variables

The difference between diffraction at HERA and at the Tevatron is that diffraction can occur not only on either p or $\bar{p}$ side as at HERA, but also on both sides. The former case is called single diffraction whereas the other one

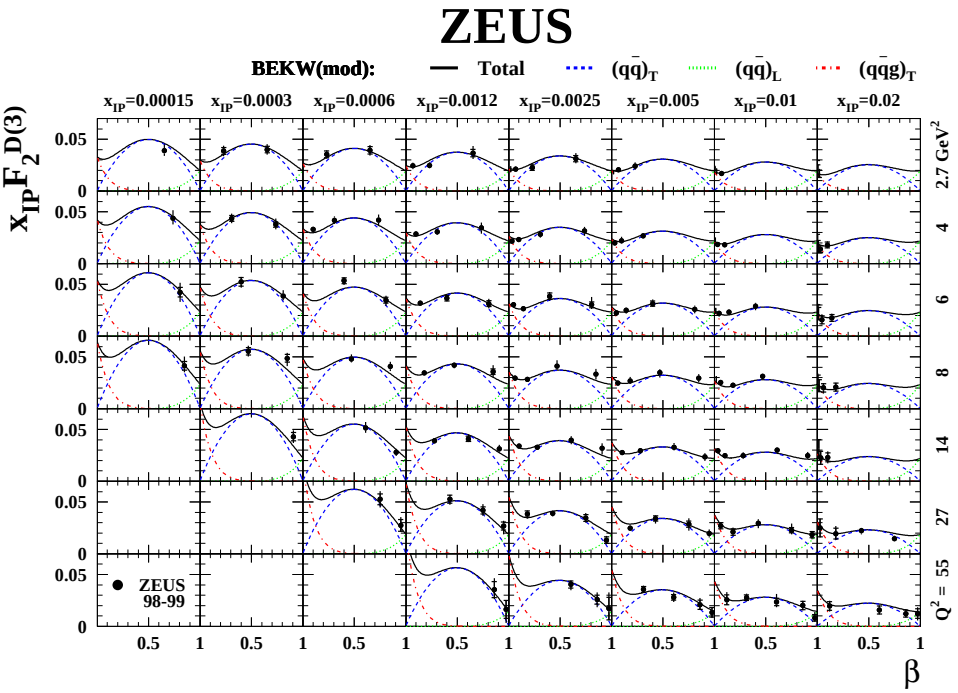

Fig. 12. Comparison between the 2 gluon model with the ZEUS M_X data.

double pomeron exchange. In the same way as we defined the kinematical variables x_P and β at HERA, we define $\xi_{1,2}(=x_P$ at HERA) as the proton fractional momentum loss (or as the p or $\bar{p}$ momentum fraction carried by the pomeron), and $\beta_{1,2}$, the fraction of the pomeron momentum carried by the interacting parton. The produced diffractive mass is equal to $M^2 = s\xi_1$ for single diffractive events and to $M^2 = s\xi_1\xi_2$ for double pomeron exchange. The size of the rapidity gap is of the order of $\Delta\eta \sim \log 1/\xi_{1,2}$.

3.2. How to find diffractive events at the Tevatron?

The selection of diffractive events at the Tevatron follows naturally from the diffractive event selection at HERA. The DØ and CDF collaborations obtained their first diffractive results using the rapidity gap method which showed that the percentage of single diffractive events was of the order of 1%, and about 0.1% for double pomeron exchanges. Unfortunately, the reconstruction of the kinematical variables is less precise than at HERA if

one uses the rapidity gap selection since it suffers from the worse resolution of reconstructing hadronic final states.

The other more precise method is to tag directly the p and $\bar{p}$ in the final state. The CDF collaboration installed roman pot detectors in the outgoing $\bar{p}$ direction only at the end of Run I [11], whereas the DØ collaboration installed them both in the outgoing p and $\bar{p}$ directions [12]. The DØ (dipole detectors) and CDF roman pots cover the acceptance of t close to 0 and $0.02 < \xi < 0.05$ in the outgoing $\bar{p}$ direction only. In addition, the DØ coverage extends for $0.5 < |t| < 1.5$ GeV^2, and $0.001 < \xi < 0.03$ in both p and $\bar{p}$ directions (quadrupole detectors). The CDF collaboration completed the detectors in the forward region by adding a miniplug calorimeter on both p and $\bar{p}$ sides allowing a coverage of $3.5 < |\eta| < 5.1$ and some beam showing counters close to beam pipe ($5.5 < |\eta| < 7.5$) allowing to reject non diffractive events.

3.3. Measurement of elastic events at DØ

Due to the high value of the production cross section, one of the first physics topics studied by the DØ collaboration was the elastic scattering cross section. Elastic events can also be used to align precisely the detectors. During its commissioning runs, the DØ collaboration was able to measure the diffractive slope for elastic events using double tagged events. The DØ results together with the results from the previous lower energy experiments are diplayed in Fig. 13. The normalisation of the DØ data is arbitrary since the data were taken using the commissioning runs of the roman pot detectors in stand-alone mode without any access to luminosity measurements. These data show the potential of the DØ roman pot detectors and this measurement will be performed again soon now that the roman pot detectors are fully included in the DØ readout system. A great challenge is to measure the change of slope in t of the elastic cross section towards 0.55-0.6 GeV^2 predicted by the models. Many measurements such as the pomeron structure in single diffractive events or double pomeron exchange, inclusive diffraction, diffractive Z, W and b-jets are being pursued in the DØ collaboration.

3.4. Factorisation or factorisation breaking at the Tevatron?

The CDF collaboration measured diffractive events at the Tevatron and their characteristics. In general, diffractive events show as expected less QCD radiation: for instance, dijet events are more back-to-back or the difference in azimuthal angles between both jets is more peaked towards π. To make predictions at the Tevatron and the LHC, it is useful to know if factorisation holds. In other words, is it possible to use the parton distri-

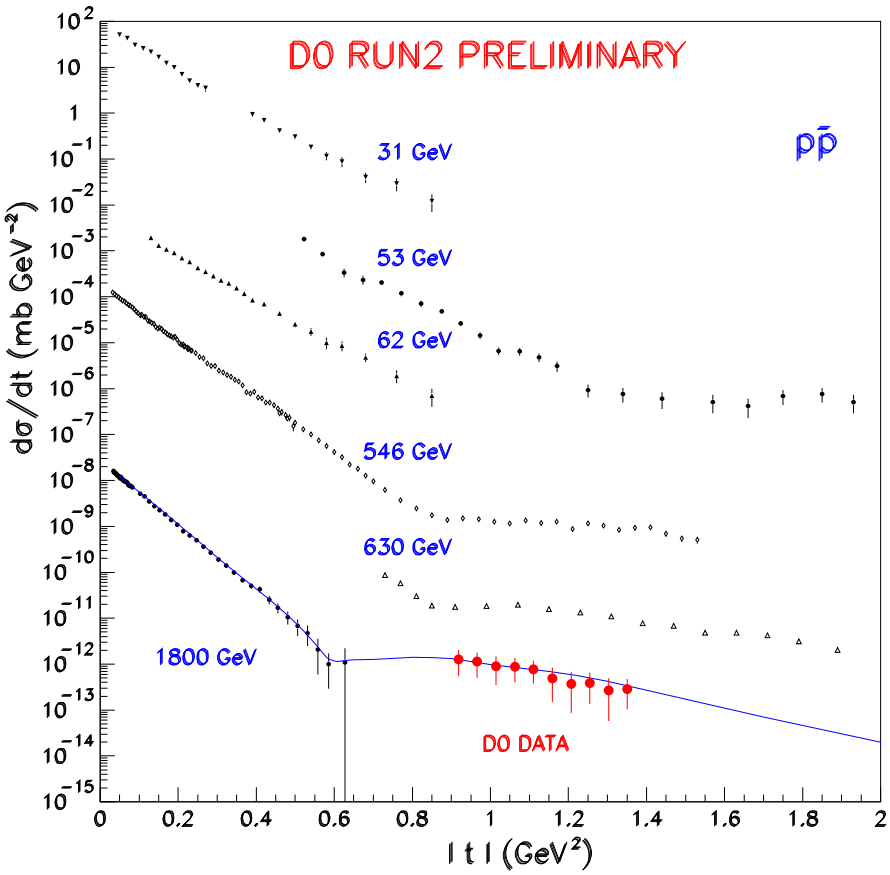

Fig. 13. Measurement of the t-slope of the elastic cross section in DØ .

butions in the pomeron obtained in the previous section using HERA data to make predictions at the Tevatron, and also further constrain the parton distribution functions in the pomeron since the reach in the diffractive kinematical plane at the Tevatron and HERA is different? Theoretically, factorisation is not expected to hold between the Tevatron and HERA due to additional pp or $p\bar{p}$ interactions. For instance, some soft gluon exchanges between protons can occur at a longer time scale than the hard interaction and destroy the rapidity gap or the proton does not remain intact after interaction. The factorisation break-up is confirmed by comparing the per-

centage of diffractive events at HERA and the Tevatron (10% at HERA and about 1% of single diffractive events at the Tevatron) showing already that factorisation does not hold. This introduces the concept of gap survival probability, the probability that there is no soft additional interaction or in other words that the event remains diffractive. We will mention in the following how this concept can be tested directly at the Tevatron.

The first factorisation test concerns CDF data only. It is interesting to check whether factorisation holds within CDF data alone, or in other words if the β and Q^2 dependence can be factorised out from the ξ one. Fig. 14 shows the percentage of diffractive events as a function of x for different ξ bins and shows the same x-dependence in all ξ bins supporting the fact that CDF data are consistent with factorisation [13]. The CDF collaboration also studied the x dependence for different Q^2 bins which lead to the same conclusions. This also shows that the Tevatron data do not require additional secondary reggeon trajectories as in H1.

The second step is to check whether factorisation holds or not between Tevatron and HERA data. The measurement of the diffractive structure function is possible directly at the Tevatron. The CDF collaboration measured the ratio of dijet events in single diffractive and non diffractive events, which is directly proportional to the ratio of the diffractive to the "standard" proton structure functions F_2:

$$R(x) = \frac{Rate_{jj}^{SD}(x)}{Rate_{jj}^{ND}(x)} \sim \frac{F_{jj}^{SD}(x)}{F_{jj}^{ND}(x)} \tag{11}$$

The "standard" proton structure function is known from the usual PDFs obtained by the CTEQ or MRST collaborations. The comparison between the CDF measurement (black points, with systematics errors as shaded area) and the expectation from the H1 QCD fits in full line is shown in Fig. 15. We notice a discrepancy of a factor 8 to 10 between the data and the predictions from the QCD fit, showing that factorisation does not hold. However, the difference is compatible with a constant on a large part of the kinematical plane in β, showing that the survival probability does not seem to be β-dependent within experimental uncertainties.

The other interesting measurement which can be also performed at the Tevatron is the test of factorisation between single diffraction and double pomeron exchange. The results from the CDF collaboration are shown in Fig. 16. The left plot shows the definition of the two ratios while the right figure shows the comparison between the ratio of double pomeron exchange to single diffraction and the QCD predictions using HERA data in full line. Whereas factorisation was not true for the ratio of single diffraction to non diffractive events, factorisation holds for the ratio of double pomeron

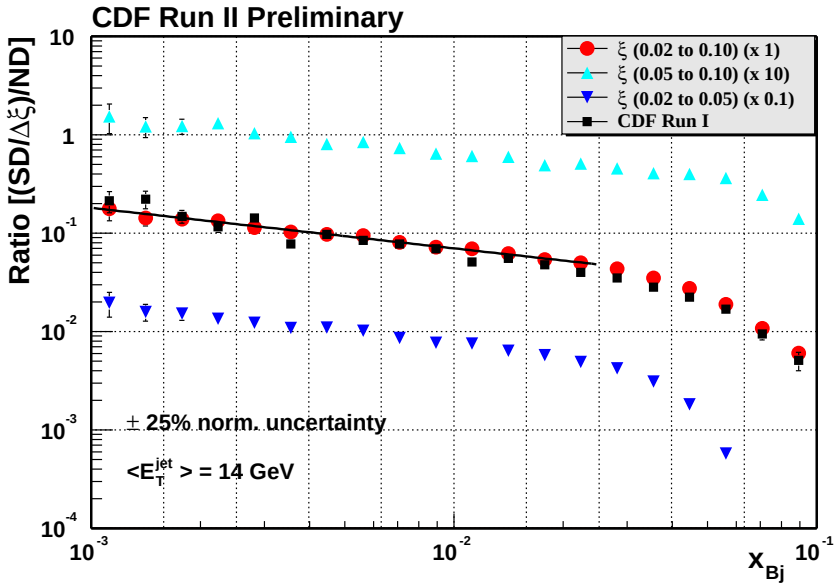

Fig. 14. Test of factorisation within CDF data alone.

exchange to single diffraction! In other words, the price to pay for one gap is the same as the price to pay for two gaps. The survival probability, i.e. the probability not to emit an additional soft gluon after the hard interaction needs to be applied only once to require the existence of a diffractive event, but should not be applied again for double pomeron exchange.

3.5. Survival probability studies in H1

We mentioned in the previous section that the concept of survival probablity is related to soft gluon emission. This process can also be studied at HERA using resolved photoproduction where events are sensitive to the hadronic structure of the photon (see Fig. 17, right plot). The resolved process is different from the direct one where the photon couples directly to the pomeron (see Fig. 17, left plot). In that case, we get an hadron hadron process like at the Tevatron since we are sensitive to the hadronic contents of the photon. In Fig. 18, we display the ratio between data and NLO predictions for DIS (red triangles) and photoproduction data (black points). We notice that we see a different of about a factor 2 between these two data sets which might be an indication of survival probability effects. However, no difference is observed between resolved or direct photoproduction where

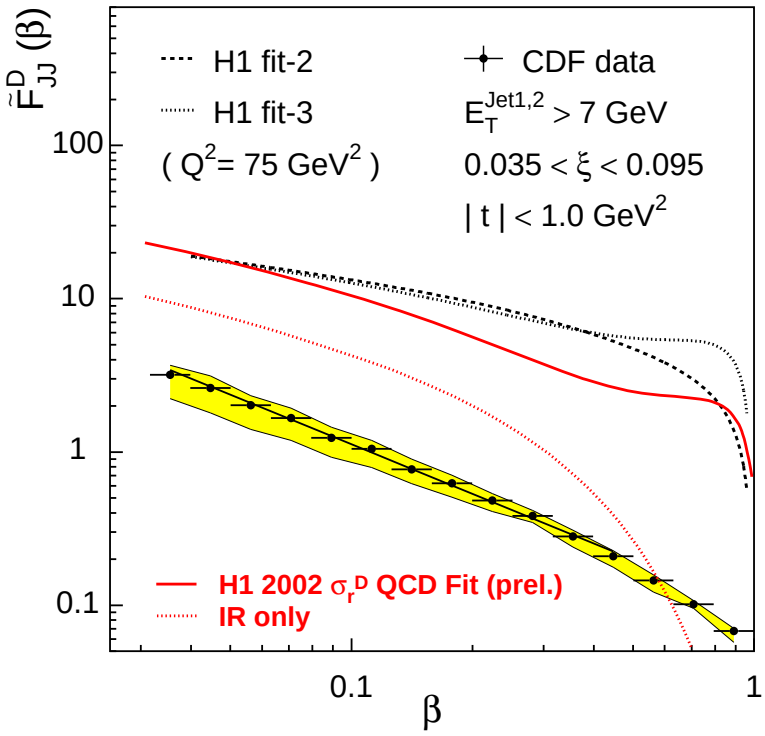

Fig. 15. Comparison between the CDF measurement of diffractive structure function (black points) with the expectation of the H1 QCD fits (red full line).

factorisation is expected to hold.

3.6. Possibility of survival probablity measurements at DØ

A new measurement to be performed at the Tevatron, in the DØ experiment has been proposed [14], which can be decisive to test directly the concept of survival probability at the Tevatron, by looking at the azimuthal distributions of the outgoing proton and antiproton with respect to the beam direction.

In Fig. 19, we display the survival probability for three different values of t as a function of the difference in azimuthal angle between the scattered

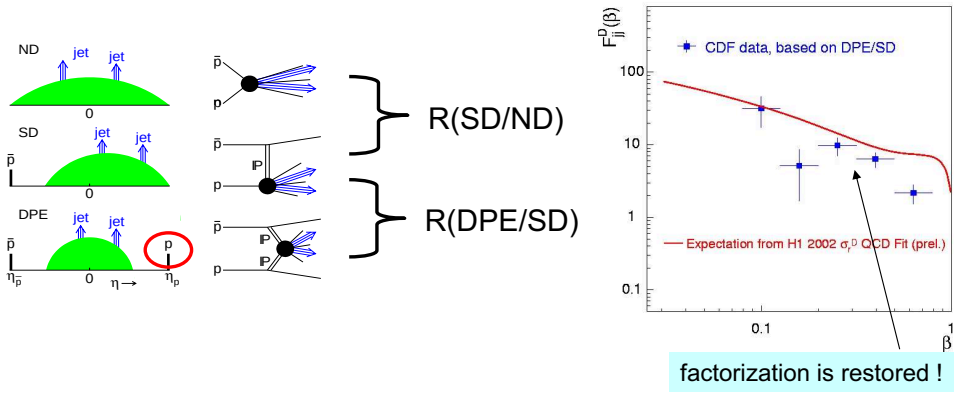

Fig. 16. Restoration of factorisation for the ratio of double pomeron exchange to single diffractive events (CDF Coll.).

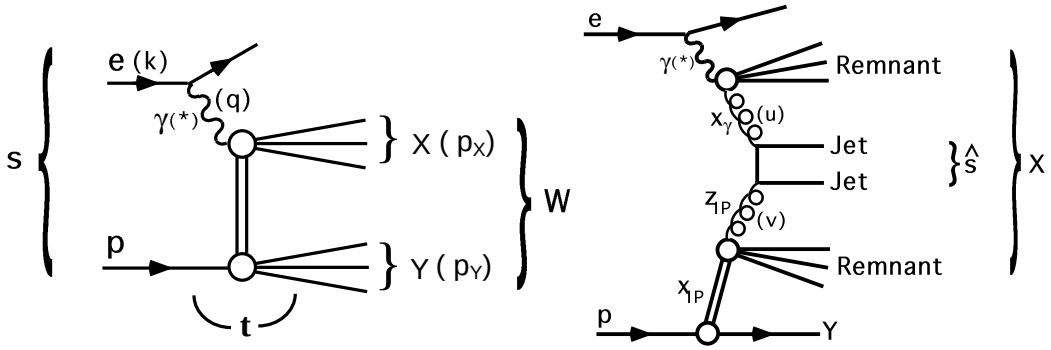

Fig. 17. Scheme of direct (left) or resolved (right) photoproduction events.

p and $\bar{p}$. The upper black curve represents the case where the t of the p and $\bar{p}$ are similar and close to 0. In that case, only a weak dependence on $\Delta\Phi$ is observed. The conclusion is different for asymmetric cases or cases when t is different from 0: Fig. 19 also shows the result in full red line for the asymmetric case ($t_1 = 0.2$, $t_2 = 0.7$ GeV^2), and in full and dashed blue lines for $t_1 = t_2 = 0.7$ GeV^2 for two different models of survival probabilities. We notice that we get a very strong $\Delta\Phi$ dependence of more than one order of magnitude.

The Φ dependence can be tested directly using the roman pot detectors

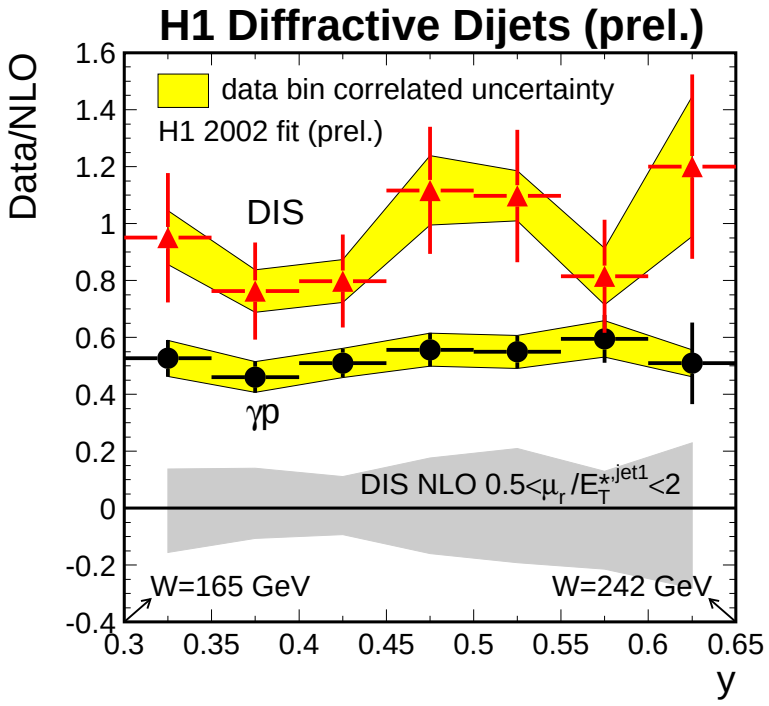

Fig. 18. Test of factorisation using photoproduction or DIS data in H1.

at DØ (dipole and quadrupole detectors) and their possibility to measure the azimuthal angles of the p and $\bar{p}$. For this purpose, we define the following configurations for dipole-quadrupole tags: same side (corresponding to $\Delta\Phi < 45$ degrees), opposite side (corresponding to $\Delta\Phi > 135$ degrees), and middle side (corresponding to $45 < \Delta\Phi < 135$ degrees). In Table 1, we give the ratios $middle/(2 \times same)$ and $opposite/same$ (note that we divide $middle$ by 2 to get the same domain size in Φ) for the different models. In order to obtain these predictions, we used the full acceptance in t and ξ of the FPD detector. Moreover the ratios for two different tagging configurations, namely for $\bar{p}$ tagged in dipole detectors, and p in quadrupoles, or for both p and $\bar{p}$ tagged in quadrupole detectors [14] were computed.

The results are also compared to expectations using another kind of model to describe diffractive events, namely soft colour interaction [15]. This model assumes that diffraction is not due to a colourless exchange at the hard vertex (called pomeron) but rather to string rearrangement in the final state during hadronisation. In this kind of model, there is a probability (to be determined by the experiment) that there is no string connection, and so no colour exchange, between the partons in the proton and the

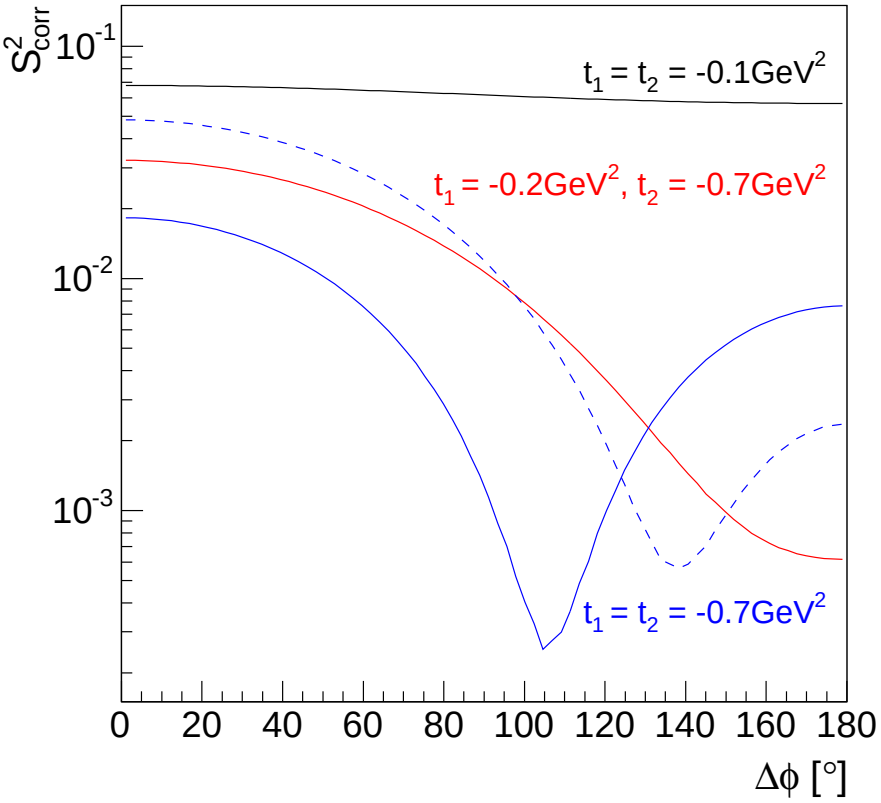

Fig. 19. $\Delta\Phi$ dependence of the survival probability for two different models of survival probability where $\Delta\Phi$ is the difference in azimuthal angle between the scattered p and $\bar{p}$ in the final state, and for three different values of t (see text).

scattered quark produced during the hard interaction. Since this model does not imply the existence of pomeron, there is no need of a concept like survival probability, and no dependence on $\Delta\Phi$ of diffractive cross sections. The proposed measurement would allow to distinguish between these two dramatically different models of diffraction.

Config.	model	midd./ same	opp./ same
Quad.	SCI	1.3	1.1
+ Dipole	Pom. 1	0.36	0.18
	Pom. 2	0.47	0.20
Quad.	SCI	1.4	1.2
+ Quad.	Pom. 1	0.14	0.31
	Pom. 2	0.20	0.049

Table 1. Predictions for a proposed measurement of diffractive cross section ratios in different regions of $\Delta\Phi$ at the Tevatron (see text for the definition of middle, same and opposite). The first (resp. second) measurement involves the quadrupole and dipole detectors (resp. quadrupole detectors only) leading to asymmetric (resp. symmetric) cuts on t.

4. Diffractive exclusive event production

4.1. Interest of exclusive events

A schematic view of non diffractive, inclusive double pomeron exchange, exclusive diffractive events at the Tevatron or the LHC is displayed in Fig. 20. The upper left plot shows the "standard" non diffractive events where the Higgs boson, the dijet or diphotons are produced directly by a coupling to the proton and shows proton remnants. The bottom plot displays the standard diffractive double pomeron exchange where the protons remain intact after interaction and the total available energy is used to produce the heavy object (Higgs boson, dijets, diphotons...) and the pomeron remnants. We have so far only discussed this kind of events and their diffractive production using the parton densities measured at HERA. There may be a third class of processes displayed in the upper right figure, namely the exclusive diffractive production. In this kind of events, the full energy is used to produce the heavy object (Higgs boson, dijets, diphotons...) and no energy is lost in pomeron remnants. There is an important kinematical consequence: the mass of the produced object can be computed using roman pot detectors and tagged protons:

$$M = \sqrt{\xi_1 \xi_2 S}. \tag{12}$$

We see immediately the advantage of those processes: we can benefit from the good roman pot resolution on ξ to get a good resolution on mass. It is then possible to measure the mass and the kinematical properties of the produced object and use this information to increase the signal over background

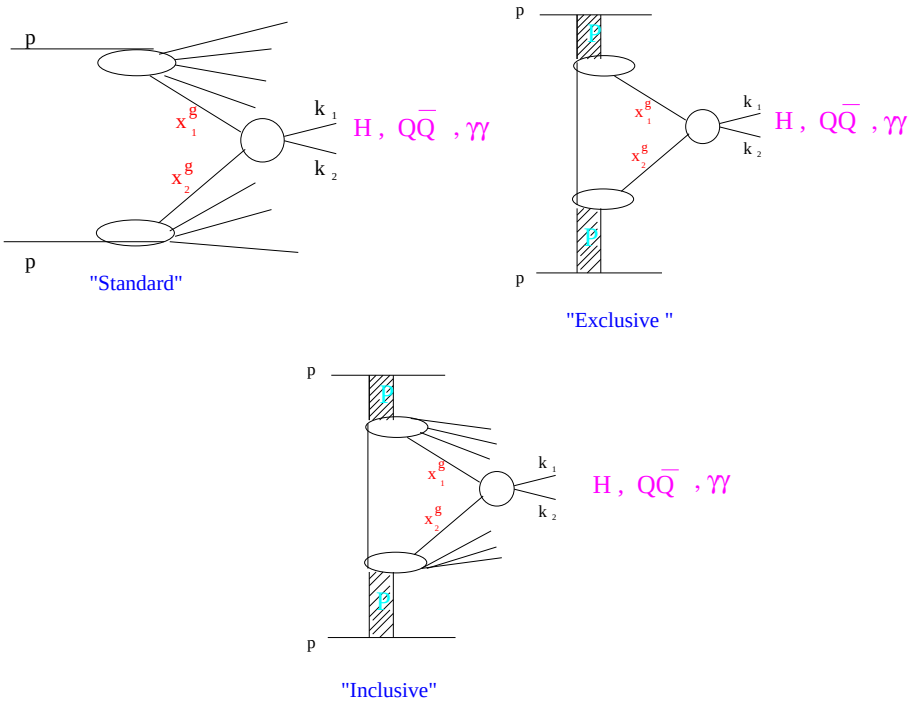

Fig. 20. Scheme of non diffractive, inclusive double pomeron exchange, exclusive diffractive events at the Tevatron or the LHC.

ratio by reducing the mass window of measurement. It is thus important to know if this kind of events exist or not.

4.2. Search for exclusive events at the Tevatron

The CDF collaboration measured the so-called dijet mass fraction in dijet events - the ratio of the mass carried by the two jets divided by the total diffractive mass - when the antiproton is tagged in the roman pot detectors and when there is a rapidity gap on the proton side to ensure that the event corresponds to a double pomeron exchange. The results are shown in Fig. 21 and are compared with the POMWIG [18] expectation using the gluon and quark densities measured by the H1 collaboration in dashed line [13]. We see a clear deficit of events towards high values of the dijet mass fraction, where exclusive events are supposed to occur (for exclusive events, the dijet mass fraction is 1 by definition at generator level and can be smeared out towards lower values taking into account the detector resolutions). Fig. 21 shows also the comparison between data and the predictions from the POMWIG

and DPEMC generators, DPEMC being used to generate exclusive events [16]. There is a good agreement between data and MC. However, this does not prove the existence of exclusive events since the POMWIG prediction shows large uncertainties (the gluon in the pomeron used in POMWIG is not the latest one obtained by the H1 collaboration [2, 6] and the uncertainty at high β is quite large as we discussed in a previous section). The results (and the conclusions) might change using the newest gluon density and will be of particular interest. In addition, it is not obvious one can use the gluon density measured at HERA at the Tevatron since factorisation does not hold, or in other words, this assumes that the survival probability is a constant, not depending on the kinematics of the interaction.

A direct precise measurement of the gluon density in the pomeron through the measurement of the diffractive dijet cross section at the Tevatron and the LHC will be necessary if one wants to prove the existence of exclusive events in the dijet channel. However, this measurement is not easy and requires a full QCD analysis. We expect that exclusive events would appear as a bump in the gluon distribution at high β, which will be difficult to interprete. To show that this bump is not due to tail of the inclusive distribution but real exclusive events, it would be necessary to show that those tails are not compatible with a standard DGLAP evolution of the gluon density in the pomeron as a function of jet transverse momentum. However, it does not seem to be easy to distinguish those effects from higher twist ones. It is thus important to look for different methods to show the existence of exclusive events.

The CDF collaboration also looked for the exclusive production of dilepton and diphoton. Contrary to diphotons, dileptons cannot be produced exclusively via pomeron exchanges since $gg \to \gamma\gamma$ is possible, but $gg \to l^+l^-$ directly is impossible. However, dileptons can be produced via QED processes, and the cross section is perfectly known. The CDF measurement is $\sigma = 1.6^{+0.5}_{-0.3}(stat) \pm 0.3(syst)$ pb which is found to be in good agreement with QED predictions and shows that the acceptance, efficiencies of the detector are well understood. Three exclusive diphoton events have been observed by the CDF collaboration leading to a cross section of $\sigma = 0.14^{+0.14}_{-0.04}(stat) \pm 0.03(syst)$ pb compatible with the expectations for exclusive diphoton production at the Tevatron.

Other searches like χ_C production and the ratio of diffractive b jets to the non diffractive ones as a function of the dijet mass fraction show further indications that exclusive events might exist but there is no definite proof until now.

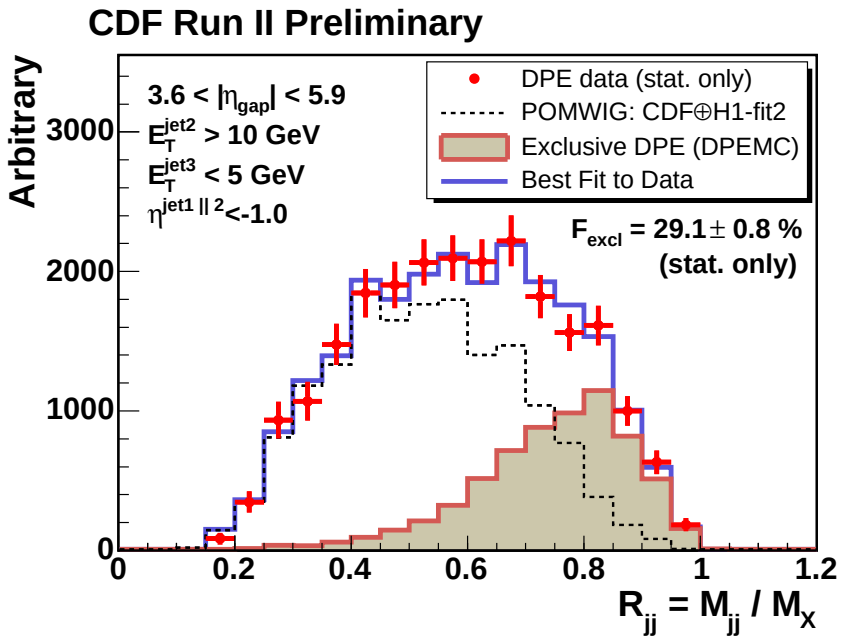

Fig. 21. Search for exclusive diffractive events at CDF.

4.3. Search for exclusive events at the LHC

The search for exclusive events at the LHC can be performed in the same channels as the ones used at the Tevatron. In addition, some other possibilities benefitting from the high luminosity of the LHC appear. One of the cleanest way to show the existence of exclusive events would be to measure the dilepton and diphoton cross section ratios as a function of the dilepton/diphoton mass. If exclusive events exist, this distribution should show a bump towards high values of the dilepton/diphoton mass since it is possible to produce exclusively diphotons but not dileptons at leading order as we mentionned in the previous paragraph.

The search for exclusive events at the LHC will also require a precise analysis and measurement of inclusive diffractive cross sections and in particular the tails at high β since it is a direct background to exclusive event production.

5. Diffraction at the LHC

In this section, we will describe briefly some projects concerning diffraction at the LHC. We will put slightly more emphasis on the diffractive

production of heavy objects such as Higgs bosons, top or stop pairs, WW events...

5.1. Diffractive event selection at the LHC

The LHC with a center-of-mass energy of 14 TeV will allow us to access a completely new kinematical domain in diffraction. So far, two experiments, namely ATLAS and CMS-TOTEM have shown interests in diffractive measurements. The diffractive event selection at the LHC will be the same as at the Tevatron. However, the rapidity gap selection will no longer be possible at high luminosity since up to 25 interactions per bunch crossing are expected to occur and soft pile-up events will kill the gaps produced by the hard interaction. Proton tagging will thus be the only possibility to detect diffractive events at high luminosity.

5.2. Measurements at the LHC using a high β^* lattice

Measurements of total cross section and luminosity are foreseen in the ATLAS [19] and TOTEM [20] experiments, and roman pots are installed at 147 and 220 m in TOTEM and 240 m in ATLAS. These measurements will require a special injection lattice of the LHC at low luminosity since they require the roman pot detectors to be moved very close to the beam. As an example, the measurement of the total cross section to be performed by TOTEM [20] is shown in Fig. 22. We notice that there is a large uncertainty on prediction of the total cross section at the LHC energy in particular due to the discrepancy between the two Tevatron measurements, and this measurement of TOTEM will be of special interest.

5.3. Hard inclusive diffraction at the LHC

In this section, we would like to discuss how we can measure the gluon density in the pomeron, especially at high β since the gluon in this kinematical domain shows large uncertainties and this is where the exclusive contributions should show up if they exist. To take into account the high-β uncertainties of the gluon distribution, we chose to multiply the gluon density in the pomeron measured at HERA by a factor $(1-\beta)^\nu$ where ν varies between -1.0 and 1.0. If ν is negative, we enhance the gluon density at high β by definition, especially at low Q^2.

A possible measurement at the LHC is described in Fig. 23. The dijet mass fraction is shown in dijet diffractive production for different jet transverse momenta ($P_T > 100$ (upper left), 200 (upper right), 300 (lower left) and 400 GeV (lower right)), and for the different values if ν. We notice

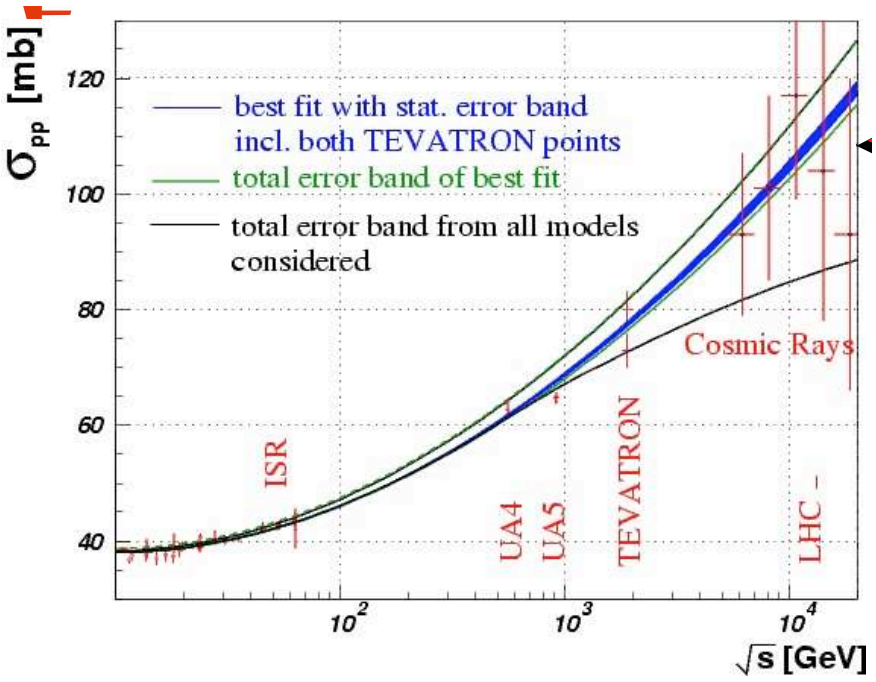

Fig. 22. Measurement of the total cross section.

that the variation of this distribution as a function of jet p_T can assess directly the high β behaviour of the gluon density. In the same kind of ideas, it is also possible to use $t\bar{t}$ event production to test the high-β gluon. Of course, this kind of measurement will not replace a direct QCD analysis of the diffractive dijet cross section measurement.

Other measurements already mentionned such as the diphoton, dilepton cross section ratio as a function of the dijet mass, the b jet, χ_C, W and Z cross section measurements will be also quite important at the LHC.

5.4. Exclusive Higgs production at the LHC

As we already mentionned in one of the previous sections, one special interest of diffractive events at the LHC is related to the existence of exclusive events. So far, two projects are being discussed at the LHC: the installation of roman pot detectors at 220 m in ATLAS [21], and at 420 m for the ATLAS and CMS collaborations [22].

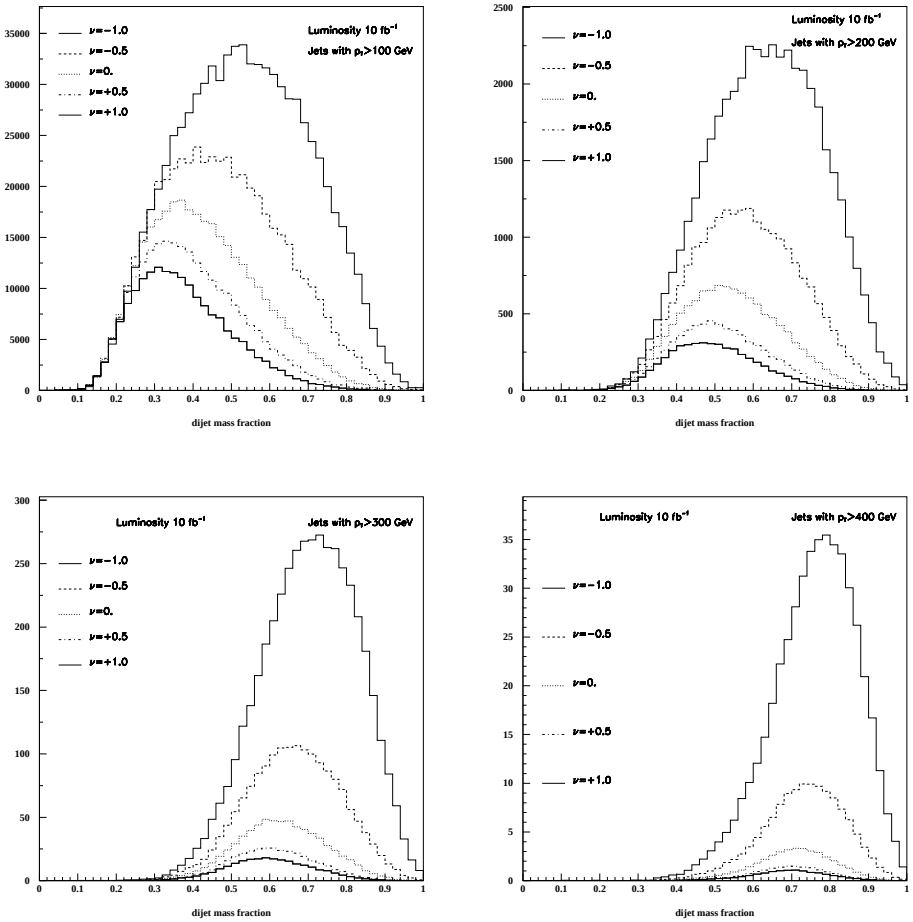

Fig. 23. Dijet mass fraction for jet $P_T > 100$ (upper left), 200 (upper right), 300 (lower left) and 400 GeV (lower right) for different gluon assumptions at high β (the gluon is multiplied by $(1-\beta)^\nu$).

The results discussed in this section rely on the DPEMC Monte Carlo to produce Higgs bosons exclusively [16, 17] and a fast simulation of a typical LHC detector (ATLAS or CMS). Results are given in Fig. 24 for a Higgs mass of 120 GeV, in terms of the signal to background ratio S/B, as a function of the Higgs boson mass resolution. Let us notice that the background is mainly due the exclusive $b\bar{b}$ production. However the tail of the inclusive $b\bar{b}$ production can also be a relevant contribution and this is

M_{Higgs}	cross section	signal	backg.	S/B	σ
120	3.9	27.1	28.5	0.95	5.1
130	3.1	20.6	18.8	1.10	4.8
140	2.0	12.6	11.7	1.08	3.7

Table 2. Exclusive Higgs production cross section for different Higgs masses, number of signal and background events for 100 fb^{-1}, ratio, and number of standard deviations (σ).

related to the high β gluon density which is badly known at present. In order to obtain a S/B of 3 (resp. 1, 0.5), a mass resolution of about 0.3 GeV (resp. 1.2, 2.3 GeV) is needed. A mass resolution of the order of 1 GeV seems to be technically feasible.

The diffractive SUSY Higgs boson production cross section is noticeably enhanced at high values of $\tan\beta$ and since we look for Higgs decaying into $b\bar{b}$, it is possible to benefit directly from the enhancement of the cross section contrary to the non diffractive case. A signal-over-background up to a factor 50 can be reached for 100 fb^{-1} for $\tan\beta \sim 50$ [23] (see Fig. 25).

5.5. Exclusive top, stop and W pair production at the LHC

In the same way that Higgs bosons can be produced exclusively, it is possible to produce W, top and stops quark pairs. WW bosons are produced via QED processes which means that their cross section is perfectly known. On the contrary, top and stop pair production are obtained via double pomeron exchanges and the production cross section is still uncertain.

The method to reconstruct the mass of heavy objects double diffractively produced at the LHC is based on a fit to the turn-on point of the missing mass distribution at threshold [24].

One proposed method (the "histogram" method) corresponds to the comparison of the mass distribution in data with some reference distributions following a Monte Carlo simulation of the detector with different input masses corresponding to the data luminosity. As an example, we can produce a data sample for 100 fb^{-1} with a top mass of 174 GeV, and a few MC samples corresponding to different top masses between 150 and 200 GeV. For each Monte Carlo sample, a χ^2 value corresponding to the population difference in each bin between data and MC is computed. The mass point where the χ^2 is minimum corresponds to the mass of the produced object in data. This method has the advantage of being easy but requires a good simulation of the detector.

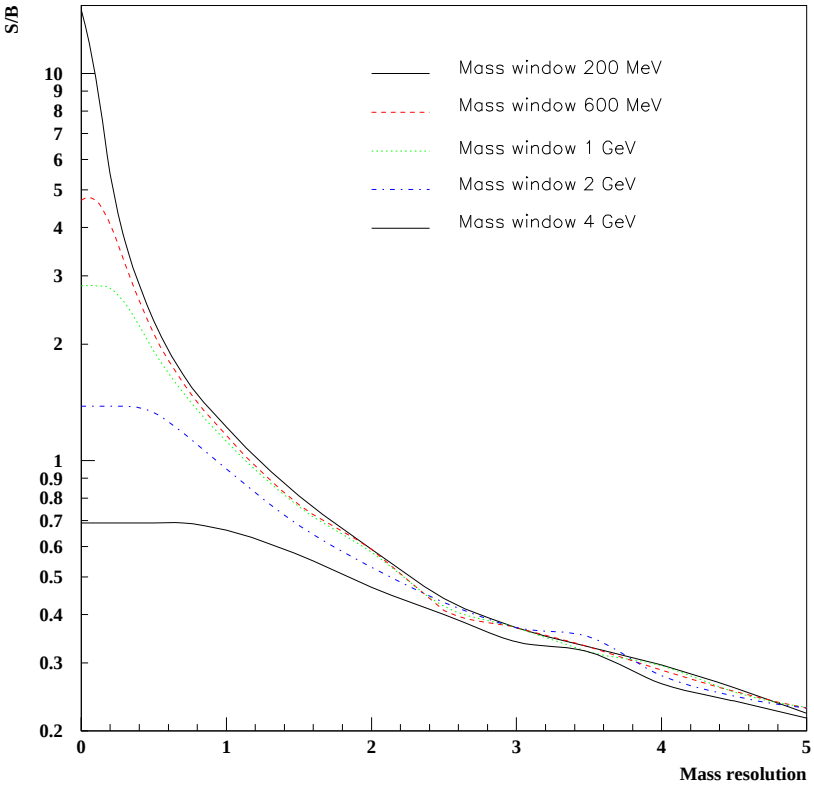

Fig. 24. Standard Model Higgs boson signal to background ratio as a function of the resolution on the missing mass, in GeV. This figure assumes a Higgs boson mass of 120 GeV.

The other proposed method (the "turn-on fit" method) is less sensitive to the MC simulation of the detectors. As mentioned earlier, the threshold scan is directly sensitive to the mass of the diffractively produced object (in the WW case for instance, it is sensitive to twice the WW mass). The idea is thus to fit the turn-on point of the missing mass distribution which leads directly to the mass of the produced object, the WW boson. Due to its robustness, this method is considered as the "default" one.

The precision of the WW mass measurement (0.3 GeV for 300 fb^{-1}) is not competitive with other methods, but provides a very precise check

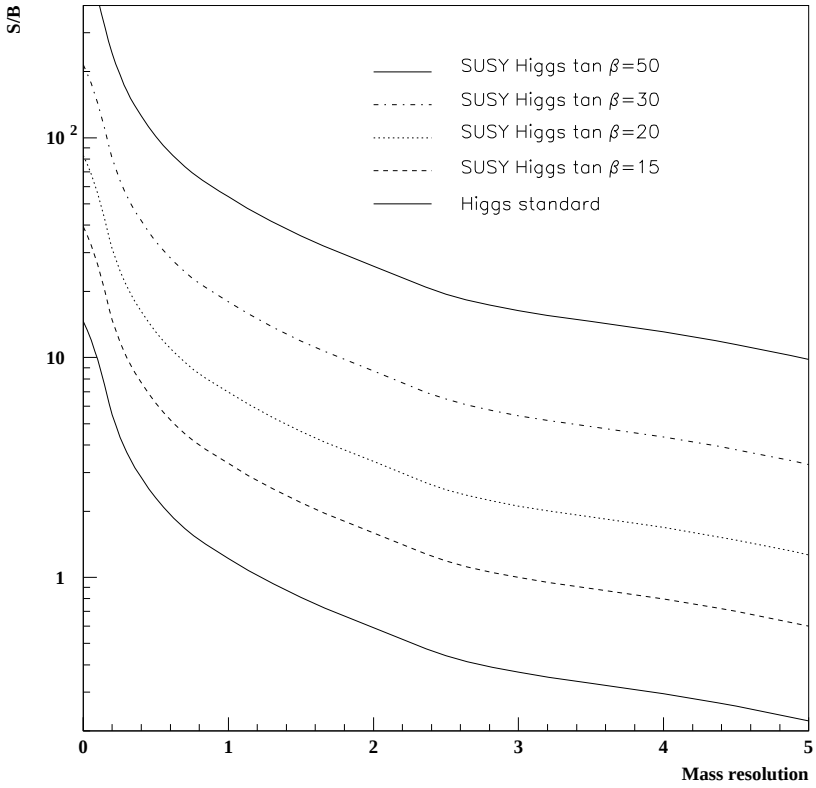

Fig. 25. SUSY Higgs boson signal to background ratio as a function of the resolution on the missing mass, in GeV. This figure assumes a Higgs boson mass of 120 GeV.

of the calibration of the roman pot detectors. WW events will also allow to assess directly the sensitivity to the photon anomalous coupling since it would reveal itself by a modification of the well-known QED WW production cross section. We can notice that the WW production cross section is proportional to the fourth power of the γW coupling which ensures a very good sensitivity of that process [25]. The precision of the top mass measurement is however competitive, with an expected precision better than 1 GeV at high luminosity provided that the cross section is high enough. The other application is to use the so-called "threshold-scan method" to measure the stop mass [23]. After taking into account the stop width, we

obtain a resolution on the stop mass of 0.4, 0.7 and 4.3 GeV for a stop mass of 174.3, 210 and 393 GeV for a luminosity (divided by the signal efficiency) of 100 fb^{-1}.

The caveat is of course that the production via diffractive exclusive processes is model dependent, and definitely needs the Tevatron and LHC data to test the models. It will allow us to determine more precisely the production cross section by testing and measuring at the Tevatron the jet and photon production for high masses and high dijet or diphoton mass fraction.

6. Conclusion

In these lectures, we presented and discussed the most recent results on inclusive diffraction from the HERA and Tevatron experiments and gave the prospects for the future at the LHC. Of special interest is the exclusive production of Higgs boson and heavy objects (W, top, stop pairs) which will require a better understanding of diffractive events and the link between ep and hadronic colliders, and precise measurements and analyses of inclusive diffraction at the LHC in particular to constrain further the gluon density in the pomeron.

Acknowledgments

I thank Robi Peschanski and Oldřich Kepka for a careful reading of the manuscript.

REFERENCES

[1] J. Collins, Phys. Rev. **D 57** (1998) 3051.

[2] H1 Collaboration, arXiv:hep-ex/0606004; H1 Collaboration, preprint hep-ex/0606003 .

[3] ZEUS Collaboration, Nucl. Phys. **B 713** (2005) 3.

[4] H1 Collaboration, preprint hep-ex/0606003 .

[5] H1 Collab., Z. Phys. **C76** (1997) 613.

[6] C. Royon, L. Schoeffel, S. Sapeta, R. Peschanski, E. Sauvan, preprint hep-ph/0609291; C. Royon, L. Schoeffel, R. Peschanski, E. Sauvan, Nucl. Phys. **B746** (2006) 15.

[7] G.Altarelli and G.Parisi, *Nucl. Phys.* **B126** 18C (1977) 298; V.N.Gribov and L.N.Lipatov, *Sov. Journ. Nucl. Phys.* (1972) 438 and 675; Yu.L.Dokshitzer, *Sov. Phys. JETP.* **46** (1977) 641.

[8] J.Bartels, J.Ellis, H.Kowalski, M.Wuesthoff, Eur.Phys.J.C7 (1999) 443, J.Bartels, C.Royon, Mod. Phys. Lett. **A14** (1999) 1583.

[9] A.H.Mueller and B.Patel, Nucl. Phys. **B425** (1994) 471; A.H.Mueller, Nucl. Phys. **B437** (1995) 107; A.H.Mueller, Nucl. Phys. **B415** (1994) 373; H.Navelet, R.Peschanski, Ch.Royon, S.Wallon, Phys. Lett. **B385** (1996) 357; A. Bialas, R.Peschanski, C.Royon, Phys. Rev. **D57** (1998) 6899; S.Munier, R.Peschanski, C.Royon, Nucl. Phys. **B534** (1998) 297.

[10] K. Golec-Biernat and M. Wusthoff, Phys. Rev. **D59** (1999) 014017; Phys. Rev. **D60** (1999) 114023.

[11] See http://www-cdf.fnal.gov.

[12] Proposal for a Forward Proton Detector at DØ , DØ Collaboration (1997), Proposal P-900 to FERMILAB PAC.

[13] M. Gallinaro, talk given at the DIS 2006 workshop, 20-24 April 2006, Tsukuba, Japan, see /http://www-conf.kek.jp/dis06/; Dino Goulianos, talk given at the low x 2006 workshop, June 28 - July 1 2206, Lisbon, Portugal, see http://www-d0.fnal.gov/ royon/lowx_lisbon

[14] A. Kupčo, R. Peschanski, C.Royon, Phys. Lett. **B606** (2005) 139, and references therein.

[15] A. Edin, G. Ingelman, J. Rathsman, Phys. Lett. **B366** (1996) 371.

[16] C. Royon, Mod. Phys. Lett. A **18**, 2169 (2003) and references therein; M. Boonekamp, R. Peschanski, C. Royon, Phys. Rev. Lett. **87** (2001) 251806 and Nucl. Phys. **B669** (2003) 277; M. Boonekamp, A. De Roeck, R. Peschanski, C. Royon, Phys. Lett. **B550** (2002) 93; V.A. Khoze, A.D. Martin, M.G. Ryskin, Eur. Phys. J. **C19** (2001) 477 and Eur. Phys. J. **C24** (2002) 581.

[17] See http://boonekam.home.cern.ch/boonekam/dpemc.htm

[18] B. Cox, J. Forshaw, Comput. Phys. Commun. **144** (2002) 104.

[19] ATLAS Coll., see http://atlas-project-lumi-fphys.web.cern.ch/atlas-project-lumi-fphys/

[20] TOTEM Coll., see http://totem.web.cern.ch/Totem/, TOTEM Technical Design Report,

[21] C. Royon, talk given at the Diffraction 2006 conference, Milos Island, Greece, 5-10 September 2006, see http://www.cs.infn.it/diff2006/.

[22] FP420 Coll., see http://www.fp420.com

[23] M. Boonekamp, J. Cammin, S. Lavignac, R. Peschanski, C. Royon, Phys. Rev. **D73** (2006) 115011, and references therein.

[24] M. Boonekamp, J. Cammin, R. Peschanski, C. Royon, preprint hep-ph/0504199.

[25] M. Boonekamp, S. Hassani, O. Kepka, R. Peschanski, C. Royon in preparation.